Analysis of 3D Deafness Effects in Highly Directional mmWave Communications

Olga Chukhno*, Nadezhda Chukhno*, Olga Galinina†,
Yuliya Gaidamaka*‡, Sergey Andreev†, and Konstantin Samouylov*‡
*Peoples' Friendship University of Russia, Rissia
{olga-chukhno, nvchukhno}@gmail.com, {gaydamaka-yuv, samuylov-ke}@rudn.ru
‡Federal Research Center "Computer Science and Control" of the Russian Academy of Sciences, Russia
†Tampere University, Finland
{olga.galinina, sergey.andreev}@tuni.fi

Abstract—In this paper, we address a problem of 3D directional deafness, which may arise for millimeter-wave (mmWave) devices, e.g., in the contention-based access period of the IEEE 802.11ad/ay protocols. To evaluate the probability of 3D deafness, we develop an analytical framework based on stochastic geometry methods. In particular, we study a minimal feasible set of devices equipped with highly directional antennas with an arbitrary antenna pattern and provide an analytical expression for the distance-dependent 3D directional deafness probability. To abstract away from particular antenna patterns, we propose an analytically tractable model of an antenna pattern that is given by a piece-wise linear function of the beamwidth. Using this tractable equation, we derive a corresponding closed-form lower bound for the deafness probability that serves as an approximation for an arbitrary antenna with the same half-power beamwidth. Finally, we study the effects of antenna settings on the deafness probability and derive a scaling law for its lower values.

Index Terms—mmWave, deafness, 3D, directional access.

I. INTRODUCTION

The most striking sign of our times is that technology is gradually infiltrating every part of human life, blurring the boundaries between the real and digital worlds. The top strategic technology trends indicated by a recent Gartner forecast [1], for example, immersive experience (AR/VR/XR) and swarms of autonomous things (robots, vehicles, drones, etc.), pose unprecedented connectivity challenges that can only be solved by the intelligent use of millimeter-wave (mmWave) spectrum.

While mmWave history itself dates back to the 1880s, only the latest advances in antenna and chipset design led to a massive cost reduction of mmWave hardware, having made possible its practical use. As such, in the last decade, following a new surge of research interest, mmWave has been claimed as one of the key components of 5G technologies, enabling blazing data rates and low latency. With the appealing advantages of the wide bandwidth and uncrowded spectrum come limitations of the mmWave propagation that result in the necessity of relying on highly directional transmissions.

To this end, all recently standardized mmWave protocols, in licensed and unlicensed bands, employ periodic beamforming procedures for efficient channel access. In particular, two of the latest WiFi standards ratified by IEEE and operating at

60GHz frequency – 802.11ad and 802.11ay [2] – require regular sector sweep procedures that align transmit antenna beams of the communicating devices, while the receive antenna training may follow within the beam refinement protocol in the subsequent data transmission interval.

The IEEE 802.11ad/ay medium access control is based on two mechanisms: scheduling data transmission in the contention-free service period (SP) and contention-based access period (CBAP) of the beacon interval (BI). The latter is inherited from the legacy IEEE 802.11 system design and based on carrier-sense multiple access with collision avoidance (CSMA/CA) where a device initiates channel sensing (CS) before accessing the medium. While CSMA mechanism performs well for omnidirectional transmission, in the case of mmWave communications, the network suffers from the so-called *directional deafness problem*, arising when a device cannot detect a busy channel due to highly directional links between other currently communicating devices.

The discussion of the directional deafness has come a long way with multiple solutions proposed on the coordination of deaf nodes [3], [4], [5], and recently in [6]. Alternatively, some works, e.g., [7], emphasize that directional deafness could also have positive effects by substantially reducing network interference. Despite increased attention to directional deafness, quantitative analytical assessment – to the best of our knowledge – has been provided only in [8], where the deafness probability was estimated for random device locations on the plane. This approach appears viable for the conventional 2D beamforming procedures that control the antenna radiation pattern in the horizontal plane. However, new 3D beamforming techniques that allow flexible beam steering in both elevation and azimuth require us to revisit the existing approach, thus, extending it to the 3D scenario.

In this paper, we deliver an analytical framework for evaluating the directional deafness probability in 3D using a stochastic geometry formulation. In particular, we study a minimal feasible set of devices equipped with highly-directional antennas with an arbitrary antenna pattern and provide an *analytical expression* for the distance-dependent 3D directional deafness probability. To abstract from particular antenna patterns, we propose an analytically tractable model of

an antenna pattern that is given by a piece-wise linear function of the beamwidth. Using this tractable expression, we derive a corresponding *closed-form lower bound* for the deafness probability that serves as an approximation for realistic antennas with the same half-power beamwidth (HPBW) and/or for the case of a Matérn hard-core point process. Importantly, our approach is applicable to an arbitrary distribution of network nodes within an arbitrary area of interest.

The remainder of this paper is organized as follows. Section II introduces the system model and details our key assumptions. In Section III, we provide an analytical solution for calculating the deafness probability in our 3D space setup and introduce the proposed antenna pattern model. Finally, selected numerical examples are provided in Section V, followed by concluding remarks.

II. SYSTEM MODEL AND ASSUMPTIONS

In this section, we introduce our system model based on the directional communication between three mmWave devices in 3D and discuss the underlying assumptions in detail.

A. Deployment considerations

We study an arbitrary radio link between two active devices A and B equipped with highly directional mmWave transceivers. The devices are located in a 3D space, and the location of B is randomly distributed within some *area of interest* around A. For simplicity, we assume that the area of interest is defined by a *sphere* of radius R_d centered at A, as illustrated in Fig. 1(a), and that the distribution of locations is *uniform*. We note that our proposed approach is not limited by any particular shape of the area of interest or distribution of locations of A and B and may be easily extended to any other 3D shape (e.g., a cuboid or a hemisphere) or to any distribution of B.
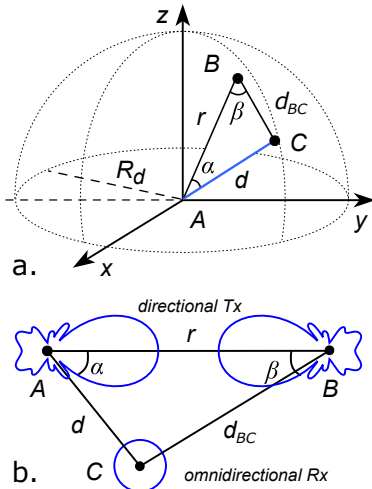

Fig. 1. Illustration of the system model in 3D space and on the plane.

Here, we refer to device B as to a *primary initiator* while device A is termed a *responder* and may act, e.g., as a mmWave access point (AP) that currently operates in the contention-based access mode. Importantly, the distance

r between the devices is random and obeys the probability density function $f_r(r)$, which in general depends on (i) the shape of the area of interest, (ii) the location of A within, and (iii) the distribution of points B. Based on the assumption of the uniform distribution of device B's location, one may easily derive the distribution of r for a sphere centered at A as

$$F_r(r) = \frac{r^3}{R_d^3} \text{ and } f_r(r) = \frac{3r^2}{R_d^3}. \tag{1}$$

Further, we consider device C as a *secondary initiator* that attempts to connect to A. Without a loss of generality, we assume that C is uniformly distributed within the sphere centered at A; however, one may also alternate these two assumptions. Here, we emphasize that our three-device setup serves as a *minimal feasible set* required for evaluating of the directional deafness probability in a system with random link deployments.

By connecting all three devices as points in a 3D space, we reduce the dimension of our problem to the 2D case, as shown in Fig. 1(b). For the sake of simplicity, we denote the angles between AB and AC or BC as α or β, respectively, while the distance between B and C is referred to as d_{BC}. Importantly, in our setup, random variables r and α are independent, while β and d_{BC} may be obtained as functions of r, α, and d.

B. Antenna abstraction

All devices transmit their data directionally, with narrow beams that are assumed to be perfectly aligned. We consider omnidirectional reception mode, which corresponds to, e.g., IEEE 802.11ad/ay operation after preliminary transmit beam training in the sector-level sweep [2].

1) General case: We assume that the antenna radiation pattern has axial symmetry with respect to the antenna boresight (the axis of the maximum radiated power), i.e., represented by a solid of revolution. This assumption allows us to incorporate the randomness of the initial degree of antenna rotation around its boresight.

Furthermore, we decompose the antenna directivity gain D into two terms: the maximum directivity D_0 along the antenna boresight, and a reduction factor capturing the decrease in antenna gain due to the angular deviation from the antenna boresight. To estimate the latter, we introduce function $\rho(\alpha) \in [0, 1]$, which scales the antenna directivity for angle $\alpha \in [0, \pi]$. The directivity gain may then be calculated as $D(\alpha) = D_0 \rho(\alpha)$, where $\rho(0) = 1$ corresponds to the antenna boresight.

The function $\rho(\alpha)$ can be (i) estimated directly from the results of radiation pattern measurements, (ii) calculated numerically for particular phased array settings, and (iii) approximated by analytically tractable models, e.g., a sector, two-sector antenna models [8], or as given below.

2) Linear approximation of directivity: Here, we propose an analytically tractable model of the antenna directivity pattern, where the maximum directivity is calculated as a ratio

between the area of a sphere and the area of a cone antenna pattern:

$$D_0 = \frac{2}{1 - \cos\frac{\theta}{2}}, \qquad (2)$$

where θ is the beamwidth, and the denominator corresponds to a solid angle of a cone with the apex angle θ. Hereinafter, we use the term antenna beamwidth to refer to the HPBW of a realistic antenna pattern that is to be approximated.

The reduction factor resulting from the angular deviation may be approximated by the following linear function:

$$\rho(\alpha) = \begin{cases} 1 - \frac{\alpha}{\theta}, & \alpha \le \theta; \\ 0, & \text{otherwise.} \end{cases} \qquad (3)$$

We note that our approximation disregards antenna side- and backlobes in contrast to, e.g., models comprising a sector and a circle of a smaller radius. However, models containing smaller circles cannot apply to the estimation of the deafness probability due to their trivial cut-off solution [8].

The proposed approximation is illustrated in Fig. 2, where we compare the linear function (3) with realistic antenna patterns for four phased antenna arrays (described further in Section IV) in both polar and Cartesian coordinate systems.
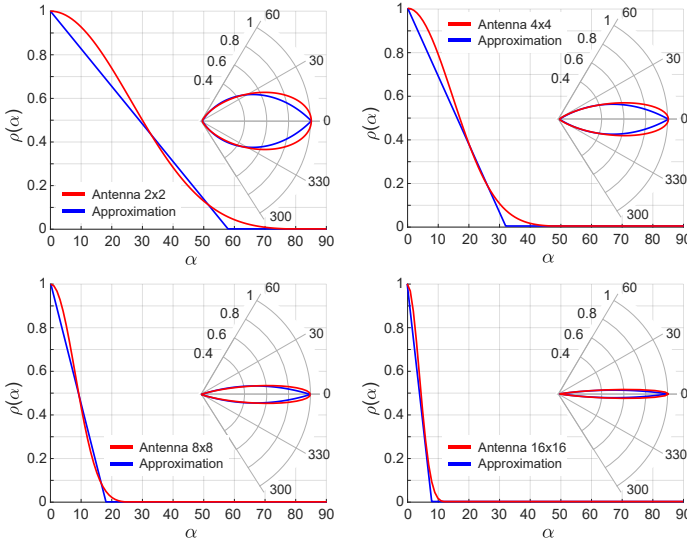

Fig. 2. Illustration of the proposed approximation (3) (blue) for uniform rectangular arrays of 2x2, 4x4, 8x8, and 16x16 elements (red).

C. Channel model and received power

We assume that the average path loss between a transmitter and a receiver obeys the following simple formula:

$$L(d) = Cd^\kappa, \qquad (4)$$

where d is the distance between two devices, C is the propagation constant, and κ is the propagation exponent. The parameters C and κ may be derived from the results of the corresponding measurement campaigns or, in the simplest line-of-sight case, taken from the Friis transmission equation as $\kappa = 2$, $C = \left(\frac{4\pi}{\lambda}\right)^2$, where λ is the wavelength.

Furthermore, let P_{tx} denote the transmit power of devices A and C; then, the received power may be found as:

$$P_{\text{rx}} = P_{\text{tx}}G_{\text{tx}}G_{\text{rx}}L^{-1}(d) = \frac{P_{\text{tx}}D_0\rho(\alpha)}{Cd^\kappa}, \qquad (5)$$

where $G_{\text{tx}} = D_0\rho(\alpha)$ is the transmit antenna gain and $G_{\text{rx}} = 1$ is the receive antenna gain in the omnidirectional reception mode.

We denote the minimum power threshold for control physical layer [2] as P_{thr}. To establish a connection or indicate a busy channel by the clear channel assessment (CCA) procedure, it is required for the device that the inequality $P_{\text{rx}} \ge P_{\text{thr}}$ holds. Here, P_{thr} defines the radius R of the coverage area, which may be derived from (5) by substituting $d = R$:

$$R = \left[\frac{P_{\text{thr}}D_0\lambda^2}{(4\pi)^2}\right]^{\frac{1}{\kappa}}. \qquad (6)$$

D. Directional deafness

We assume that devices A and B are connected and actively exchange data during an allocated CBAP when device C attempts to connect to A and performs CCA. In this case, C may encounter two possible outcomes:

1) Device C detects the signal from either of the devices (i.e., receives power $P_{\text{rx, A}} \ge P_{\text{thr}}$ from A or $P_{\text{rx, B}} \ge P_{\text{thr}}$ from B. In this case, C sets a timer and waits for the connection between A and B to be terminated, after which C resumes its connection attempts.

2) Device C does not detect transmission of either of devices A and B, i.e., both receive powers $P_{\text{rx,A}}$ and $P_{\text{rx,B}}$ at C from A and B, respectively, do not exceed the minimum threshold. Then, we refer to the situation where $P_{\text{rx, A}} < P_{\text{thr}}, P_{\text{rx,B}} < P_{\text{thr}}$ as to deafness.

The probability of the latter in the case of arbitrary locations of devices is of particular interest from the network perspective and is addressed below.

III. DEAFNESS PROBABILITY

In this section, we formulate three consecutive propositions, which correspond to general distributions of r and α and a particular case of the uniform distribution of device B's locations in a sphere centered at A. For both cases, we provide analytical solutions that could be calculated numerically. In addition, for our particular case, we also derive a closed-form lower bound on the directional deafness probability.

A. Distance-dependent deafness probability

Let us consider distributions $f_\alpha(\alpha)$ and $f_r(r)$ of the angle α and the distance between responder A and primary initiator B, correspondingly. Then, we may formulate the following proposition.

Proposition 1. For a fixed distance d between responder A and secondary initiator C, and radius of the area of interest R_d, the probability of deafness can be calculated as follows:

$$P_D(d) = \int_0^\pi\int_0^{R_d} I\left(\rho(\alpha) < \frac{d^2}{R^2}, \rho(\beta) < \frac{d_{BC}^2}{R^2}\right) f_r(r)f_\alpha(\alpha)\,dr\,d\alpha, \qquad (7)$$

where $d_{BC} = \sqrt{r^2 + d^2 - 2rd\cos\alpha}$, $\beta = \arccos\frac{r-d\cos\alpha}{d_{BC}}$ follow from the triangle, R is the coverage radius (6), and $I(A)$ is an indicator function of event A.

Proof. The proof is based on transforming inequalities $P_{\text{rx,A}} < P_{\text{thr}}$, $P_{\text{rx}} < P_{\text{thr,B}}$ similar to [8] and, therefore, is omitted here for brevity. $\square$

B. PDF $f(\alpha)$: uniform distribution of devices in a sphere

If the distribution of locations of devices B and C is uniform within the sphere of radius R_d centered at A, then the distribution of α can be established as suggested in [9]:

$$f_\alpha(\alpha) = \frac{1}{\sqrt{\pi}}\frac{\Gamma(\frac{n}{2})}{\Gamma(\frac{n-1}{2})}\sin^{n-2}\alpha, \alpha \in [0,\pi], \quad (8)$$

where n is the dimension of the space. For the 2D case, $f_\alpha(\alpha)$ is the uniform density over the interval $[0,\pi]$, and $f_\alpha(\alpha) = 1/\pi$. In our 3D case, distribution $f_\alpha(\alpha)$ transforms into:

$$f_\alpha(\alpha) = \frac{\sin\alpha}{2}, \alpha \in [0,\pi]. \quad (9)$$

Proposition 2. If locations of device B are uniformly distributed within a sphere centered at A, i.e., distances r and angles α follow the distributions (1) and (9), correspondingly, then the probability of deafness can be obtained as

$$P_D(d) = \frac{3}{2R_d^3}\int\limits_0^{\pi R_d}\!\!\!\int I\left(\rho(\alpha) < \frac{d^2}{R^2}, \rho(\beta) < \frac{d_{BC}^2}{R^2}\right)r^2\sin\alpha\, dr d\alpha, (10)$$

Proof. Follows from Proposition 1. $\square$

C. Particular case: linear model of directivity pattern

Here, we consider the antenna pattern model introduced in Section II, and for this particular case derive a closed-form expression for a lower bound of $P_D(d)$ (10).

Proposition 3. Let locations of device B be uniformly distributed within a sphere centered at A. Then, for a fixed distance d, we may establish a *lower bound* on the deafness probability as

$$P_D(d|d \le R_d\sin\theta) = \frac{d^3\cot\theta}{32R_d^3\sin^2\theta}\left[-\sin(6\theta - \frac{4d^2\theta}{R^2}) + \right.$$

$$2\sin(4\theta - \frac{2d^2\theta}{R^2}) + 4\sin(2\theta - \frac{d^2 2\theta}{R^2}) + \sin(4\theta - \frac{d^2 4\theta}{R^2}) +$$

$$\left.\sin(-2 + \frac{4d^2\theta}{R^2}) - 2\sin(\frac{2\theta d^2}{R^2}) - 12\theta + 6\pi + \frac{12\theta d^2}{R^2}\right] \quad (11)$$

or

$$P_D(d|d > R_d\sin\theta) = \frac{\cos\tilde{z}_1 - \cos\tilde{z}_2}{2} + \frac{d^3\cot\theta}{64R_d^3\sin^3\theta}\left[12\cos\theta\right.$$

$$[(\frac{d^2\theta}{R^2} - \theta + \tilde{z}_1) + (\frac{d^2\theta}{R^2} - \theta - \tilde{z}_2 + \pi)] + 6[\sin(3\theta - \frac{2d^2\theta}{R^2}) -$$

$$\sin(\frac{2d^2\theta}{R^2} - \theta) - \sin(\theta + 2\tilde{z}_1) + \sin(\theta + 2\tilde{z}_2)] + 2[\sin(5\theta -$$

$$\frac{2d^2\theta}{R^2}) - \sin(3\theta + 2\tilde{z}_1) - \sin(\frac{4d^2\theta}{R^2} + 2\theta^2) + \sin(3\theta + 2\tilde{z}_2) +$$

$$\sin(3\theta + 4\tilde{z}_1) - \sin(7\theta - \frac{4d^2\theta}{R^2}) + \sin(\frac{4d^2\theta}{R^2} - \theta) - \sin(3\theta + 4\tilde{z}_2)\right], \quad (12)$$

where $\tilde{z}_1 = \max\{\theta(1 - \frac{d^2}{R^2}), z_1\}$, $\tilde{z}_2 = \min\{\pi - \theta(1 - \frac{d^2}{R^2}), z_2\}$, and z_1, z_2 are given below by (19).

Proof. Based on (3), the probability of deafness (10) for fixed α and r can be transformed into

$$P_D(d|\alpha, r) = \Pr\left(\alpha > \theta\left(1 - \frac{d^2}{R^2}\right), \beta > \theta\left(1 - \frac{d_{BC}^2}{R^2}\right)\right). \quad (13)$$

For convenience, we split (13) into two parts as follows:

$$P_D(d|\alpha, r) = \Pr\left(\alpha > \theta(1 - \frac{d^2}{R^2}), \beta > \theta\right) +$$

$$\Pr\left(\alpha > \theta(1 - \frac{d^2}{R^2}), \theta(1 - \frac{d_{BC}^2}{R^2}) < \beta \le \theta\right). \quad (14)$$

Let us consider the first term, which in general contributes more to the total deafness probability, and continue by:

$$P_D^{(1)}(d|\alpha, r) = \Pr\left(\alpha > \theta(1 - \frac{d^2}{R^2}), \frac{r - d\cos\alpha}{d_{BC}} < \cos\theta\right). \quad (15)$$

Expanding d_{BC}, we observe that

$$\frac{r - d\cos\alpha}{d_{BC}} < \cos\theta \Longleftrightarrow 0 < r < d(\cos\alpha + \sin\alpha\cot\theta). \quad (16)$$

For $\cos\alpha + \sin\alpha\cot\theta > 0$, we rewrite $P_D^{(1)}(d|\alpha, r)$ as

$$\Pr\left(\theta(1 - \frac{d^2}{R^2}) < \alpha < \pi - \theta(1 - \frac{d^2}{R^2}), r < d(\cos\alpha + \sin\alpha\cot\theta)\right). \quad (17)$$

The function $z(\alpha) = d(\cos\alpha + \sin\alpha\cot\theta)$ may exceed the maximum value R_d, which is defined for r. Hence, we split (17) into two parts and rewrite $P_D^{(1)}(d|\alpha, r)$ as follows:

$$P_D^{(1)}(d|\alpha, r) = \Pr\left(\theta(1 - \frac{d^2}{R^2}) < \alpha < \pi - \theta(1 - \frac{d^2}{R^2}), z(\alpha) \ge \frac{R_d}{d}\right) +$$

$$\Pr\left(\theta(1 - \frac{d^2}{R^2}) < \alpha < \pi - \theta(1 - \frac{d^2}{R^2}), r < dz(\alpha), z(\alpha) < \frac{R_d}{d}\right). \quad (18)$$
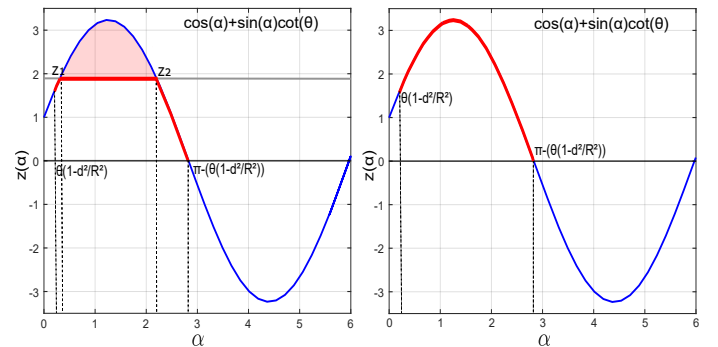
Fig. 3. Illustration of $z(a)$: the left plot shows the case of $d > R_d\sin\theta$, the right one corresponds to $d \le R_d\sin\theta$.

To solve the inequality $z(\alpha) < R_d/d$, we calculate the roots of the equation $\cos\alpha + \sin\alpha\cot\theta = \frac{R_d}{d}$ as

$$z_{1,2} = \pm 2\arctan\left[\frac{\sqrt{-\frac{R_d^2}{d^2}\tan^2\theta + \tan^2\theta + 1} \pm 1}{(\frac{R_d}{d} + 1)\tan\theta}\right]. \quad (19)$$

The function $z(\alpha)$ reaches its maximum at the point $\left(\frac{\pi}{2}-\theta, \frac{1}{\sin\theta}\right)$, as shown in the left part of Fig. 3. Hence, for $d > R_d \sin\theta$, $z(\alpha)$ exceeds the threshold $\frac{R_d}{d}$ if α falls into the interval $\left(\max\{\theta(1-\frac{d^2}{R^2}), z_1\}, \min\{\pi - \theta(1-\frac{d^2}{R^2}), z_2\}\right)$. Hence, if $d > R_d \sin\theta$, the first term in (18) may be rewritten as

$$\Pr\left(\theta(1-\tfrac{d^2}{R^2}) < \alpha < \pi - \theta(1-\tfrac{d^2}{R^2}), z(\alpha) \geq \tfrac{R_d}{d}\right) =$$
$$\tfrac{1}{2}\int_{\tilde{z}_1}^{\tilde{z}_2} \sin\alpha \, d\alpha = \tfrac{1}{2}(\cos\tilde{z}_1 - \cos\tilde{z}_2),$$

where $\tilde{z}_1 = \max\{\theta(1-\frac{d^2}{R^2}), z_1\}, \tilde{z}_2 = \min\{\pi - \theta(1-\frac{d^2}{R^2}), z_2\}$. For the second term in (18) and $d > R_d \sin\theta$, we obtain

$$\Pr\left(\theta(1-\tfrac{d^2}{R^2}) < \alpha < \pi - \theta(1-\tfrac{d^2}{R^2}), r < dz(\alpha), z(\alpha) < \tfrac{R_d}{d}\right) =$$
$$\tfrac{d^3}{2R_d^3}\int_{\theta(1-\frac{d^2}{R^2})}^{\tilde{z}_1}(\cos\alpha + \sin\alpha\cot\theta)^3 \sin\alpha \, d\alpha +$$
$$\tfrac{d^3}{2R_d^3}\int_{\tilde{z}_2}^{\pi-\theta(1-\frac{d^2}{R^2})}(\cos\alpha + \sin\alpha\cot\theta)^3 \sin\alpha \, d\alpha =$$
$$\tfrac{d^3\cot\theta}{64R_d^3\sin^3\theta}\Bigg[12\cos\theta((\tfrac{d^2\theta}{R^2}-\theta)+\tilde{z}_1) - \sin(7\theta - \tfrac{4d^2\theta}{R^2}) +$$
$$6\sin(3\theta - \tfrac{2d^2\theta}{R^2}) + 2\sin(5\theta - \tfrac{2d^2\theta}{R^2}) - 6\sin(\theta + 2\tilde{z}_1) -$$
$$2\sin(3\theta + 2\tilde{z}_1) + \sin(3\theta + 4\tilde{z}_1) + 12\cos\theta(\tfrac{d^2\theta}{R^2}-\theta-\tilde{z}_2+\pi) -$$
$$6\sin(\tfrac{2d^2\theta}{R^2}-\theta) + \sin(\tfrac{4d^2\theta}{R^2}-\theta) - 2(\sin\tfrac{4d^2\theta}{R^2}+2\theta^2) +$$
$$6\sin(\theta + 2\tilde{z}_2) + 2\sin(3\theta + 2\tilde{z}_2) - \sin(3\theta + 4\tilde{z}_2)\Bigg].$$
$$(20)$$

By collecting both terms, we obtain for $d > R_d \sin\theta$:

$$P_D^{(1)}(d|d > R_d\sin\theta) =$$
$$\Pr\left(\theta(1-\tfrac{d^2}{R^2}) < \alpha < \pi - \theta(1-\tfrac{d^2}{R^2}) - \theta, r < dz(\alpha), z(\alpha) \geq \tfrac{R_d}{d}\right) +$$
$$\Pr\left(\theta(1-\tfrac{d^2}{R^2}) < \alpha < \pi - \theta(1-\tfrac{d^2}{R^2}) - \theta, r < dz(\alpha), z(\alpha) < \tfrac{R_d}{d}\right) =$$
$$\tfrac{\cos\tilde{z}_1 - \cos\tilde{z}_2}{2} + \tfrac{d^3\cot\theta}{64R_d^3\sin^3\theta}\Bigg[12\cos\theta((\tfrac{d^2\theta}{R^2}-\theta)+\tilde{z}_1) - \sin(7\theta -$$
$$\tfrac{4d^2\theta}{R^2}) + 6\sin(3\theta - \tfrac{2d^2\theta}{R^2}) + 2\sin(5\theta - \tfrac{2d^2\theta}{R^2}) - 6\sin(\theta + 2\tilde{z}_1) -$$
$$2\sin(3\theta + 2\tilde{z}_1) + \sin(3\theta + 4\tilde{z}_1) + 12\cos\theta((\tfrac{d^2\theta}{R^2}-\theta)-\tilde{z}_2+\pi) -$$
$$6\sin(\tfrac{2d^2\theta}{R^2}-\theta) + \sin(\tfrac{4d^2\theta}{R^2}-\theta) - 2(\sin\tfrac{4d^2\theta}{R^2}+2\theta^2) +$$
$$6\sin(\theta + 2\tilde{z}_2) + 2\sin(3\theta + 2\tilde{z}_2) - \sin(3\theta + 4\tilde{z}_2)\Bigg].$$

In the case $d \leq R_d \sin\theta$, the line $\frac{R_d}{d}$ is located above the curve corresponding to $z(\alpha)$; hence, no real roots exist (see the right part of Fig. 3). Therefore, for $d \leq R_d \sin\theta$, we may produce the following:

$$P_D^{(1)}(d|d \leq R_d\sin\theta) = \tfrac{d^3}{2R_d^3}\int_{\theta(1-\frac{d^2}{R^2})}^{\pi-\theta(1-\frac{d^2}{R^2})}(\cos\alpha + \sin\alpha\cot\theta)^3 \sin\alpha \, d\alpha =$$
$$\tfrac{d^3}{32R^2R_d^3}\tfrac{\cot\theta}{\sin^2\theta}\Bigg[-R^2\sin(6\theta - \tfrac{4d^2\theta}{R^2}) + 2R^2\sin(4\theta - \tfrac{2d^2\theta}{R^2}) +$$
$$4R^2\sin(2\theta - \tfrac{d^22\theta}{R^2}) + R^2\sin(4\theta - \tfrac{d^24\theta}{R^2}) + R^2\sin(-2 + \tfrac{4d^2\theta}{R^2}) -$$
$$2R^2\sin(\tfrac{2\theta d^2}{R^2}) + 12\theta d^2 - 12\theta R^2 + 6\pi R^2\Bigg].$$

We continue by considering the second component $P_D^{(2)}(d)$ of $P_D(d)$ in (14), for which the condition $\theta(1-\frac{d_{BC}^2}{R^2}) < \beta \leq \theta$ can be rewritten as

$$r < d\left(\cos\alpha + \frac{\sin\alpha\cos(\theta - \frac{d^2\theta\sin^2\alpha}{R^2\sin^2(\theta - \frac{d^2\theta}{R^2})})}{\sin(\theta - \frac{d^2\theta}{R^2})}\right). \quad (21)$$

To solve inequality (21), one needs to find the roots of the corresponding transcendental equation. Although some expressions in the equation can be approximated by simpler alternatives, the process of obtaining the sought roots remains cumbersome. However, due to the fact that $P_D^{(2)}(d) > 0$, we conclude that $P_D(d) > P_D^{(1)}(d)$ and, thus, $P_D^{(1)}(d)$ constitutes a lower bound for the deafness probability given by (10). $\square$

IV. NUMERICAL RESULTS AND CONCLUSIONS

In this section, we provide selected numerical results on evaluating the effects of 3D directional deafness in our mmWave system. As a representative scenario, we consider the operation of a drone swarm that communicates via the IEEE 802.11ad protocol at 60 GHz (λ=0.5 cm). By default, we assume uniform rectangular phased antenna arrays that comprise isotropic elements. The transmit power is fixed across the entire fleet at the level of $P_{tx} = 23$ dBm, while $P_{thr} = -78$ dBm [2].
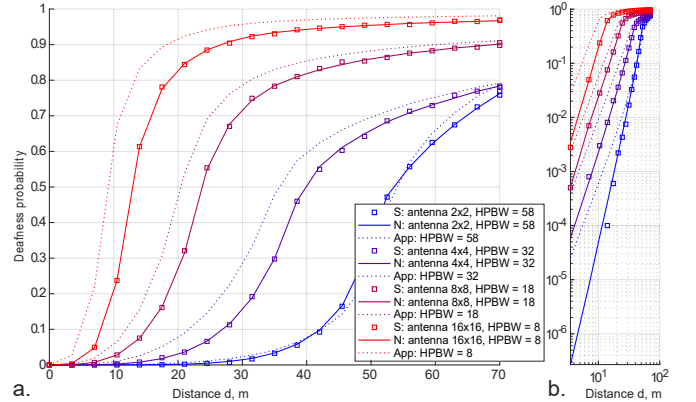
Fig. 4. Deafness probability vs. d for the approximation ("App") by the linear model (3) and realistic antenna patterns (numerical solution, "N", and simulation, "S") in both linear and logarithmic scales.

We begin by comparing the simulation results with the exact numerical solution for the deafness probability $P_D(d)$ given in (10) for the cases of (i) radiation patterns of uniform rectangular phased antenna arrays and (ii) our proposed linear model (3) for the beam pattern. As shown in Fig. 4a, the linear model represents an adequate approximation – from the deafness probability perspective – for wider beams (see, e.g., HPBW $\theta = 58$); for higher directivity, it repeats the behavior of a particular realistic antenna pattern and converges with the growing distance d between A and C. This deviation for narrower beams stems from more substantial variation in antenna pattern shapes due to a wide range of realistic settings and parameters.
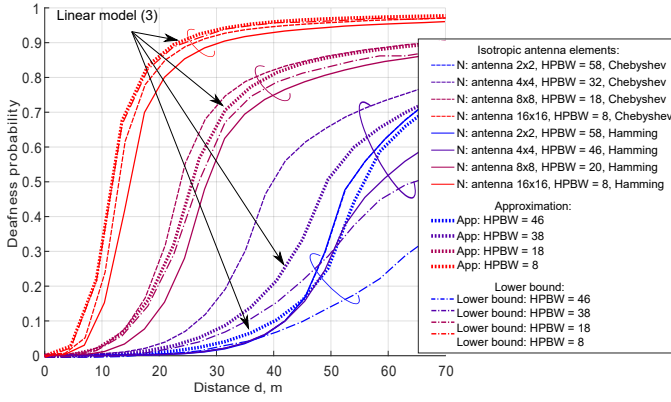
Fig. 5. Variation in the deafness probability for different antenna settings: isotropic antenna elements, Hamming/Chebyshev tapering.
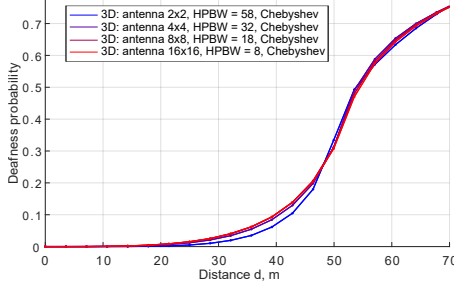

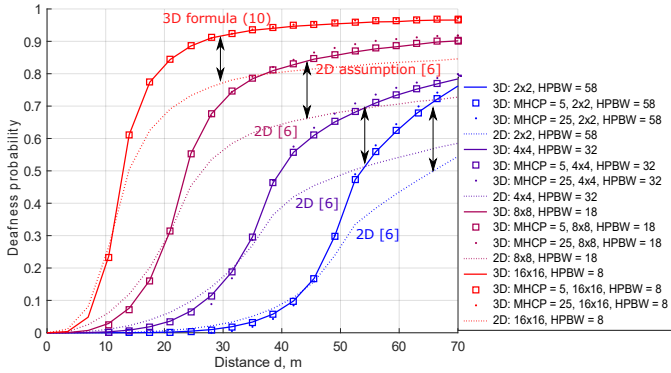Fig. 6. Effects of scaling on the deafness probability.

Fig. 7. Comparison of the deafness probability for the 2D/3D cases and different values of the MHCP parameter.

To illustrate the behavior of our linear model for lower values of $P_D(d)$, we reproduce the plots in a logarithmical scale (see Fig. 4b). When the deafness probability drops below 10^{-6}, even though the model might diverge from the realistic antenna plot by up to two orders of magnitude, it preserves the linearity of the deafness probability logarithm, which translates into the scaling law $P_D(d) \sim ad^b$, where b is defined by the slope of linear segments in Fig. 4b.

Furthermore, Fig. 5 illustrates the behavior of $P_D(d)$ and the obtained lower bound, e.g., in the case of realistic arrays of isotropic antenna elements and Chebyshev/Hamming tapering. The linear model (3) yields a reasonable approximation, and thus, could be used when the type of an antenna element is not essential for the system analysis. Its lower bound remains close for narrower beams and for cosine antenna elements, analysis of which is omitted here due to the space limitations. In addition, Fig. 6 demonstrates that scaling the system – when the radius R_d changes proportionally to the coverage R –

eliminates the gap between different values of beamwidth.

Finally, to account for the minimum allowed distance between devices, we simulate locations according to the Matérn hard-core point process of type-1 (MHCP-1) with the parameter r_{M} (i.e., distances r, d, d_{BC} between the devices do not exceed r_{M}). As seen in Fig. 7, the parameter r_{M} has a limited effect on the results. Hence, we conclude that the proposed analytical approach also provides a decent approximation for more realistic distributions of device locations. Here, we also notice a substantial difference between 3D directional deafness and the corresponding analytical results obtained under the assumption of a 2D scenario [8].

In summary, we emphasize that deafness represents a crucial challenge for any highly-directional system and may lead to detrimental effects on communication performance as we demonstrate previously in [8]. Taking into consideration more realistic 3D spatial distributions of devices yields more precise (up to 30 %) estimates for the directional deafness, whereas a simple analytically tractable directivity model may be employed as a reasonable approximation for various antenna setups and Matérn hard-core based user distribution.

REFERENCES

[1] D. Cearley and B. Burke, "Top 10 Strategic Technology Trends for 2019: A Gartner Trend Insight Report," March 2019.

[2] IEEE 802.11 Working Group, "Wireless LAN Medium Access Control (MAC) and Physical Layer (PHY) Specifications. Amendment 3: Enhancements for Very High Throughput in the 60 GHz Band," 2012.

[3] H. Gossain, C. Cordeiro, D. Cavalcanti, and D. P. Agrawal, "The deafness problems and solutions in wireless ad hoc networks using directional antennas," in *IEEE Global Telecommunications Conference Workshops, 2004. Globecom Workshops 2004.*, pp. 108–113, IEEE, 2004.

[4] T. Nitsche, C. Cordeiro, A. B Flores, E. W. Knightly, E. Perahia, and J. Widmer, "IEEE 802.11ad: directional 60 GHz communication for multi-Gigabit-per-second Wi-Fi," *IEEE Communications Magazine*, vol. 52, no. 12, pp. 132–141, 2014.

[5] G. H. Sim, T. Nitsche, and J. C. Widmer, "Addressing MAC layer inefficiency and deafness of IEEE 802.11ad millimeter wave networks using a multi-band approach," in *2016 IEEE 27th Annual International Symposium on Personal, Indoor, and Mobile Radio Communications (PIMRC)*, pp. 1–6, IEEE, 2016.

[6] V. Petrov, G. Fodor, J. Kokkoniemi, D. Moltchanov, J. Lehtomaki, S. Andreev, Y. Koucheryavy, M. Juntti, and M. Valkama, "On unified vehicular communications and radar sensing in millimeter-wave and low terahertz bands," *IEEE Wireless Communications*, 2019.

[7] S. Singh, R. Mudumbai, and U. Madhow, "Interference analysis for highly directional 60-GHz mesh networks: The case for rethinking medium access control," *IEEE/ACM Transactions on Networking (TON)*, vol. 19, no. 5, pp. 1513–1527, 2011.

[8] O. Galinina, A. Pyattaev, K. Johnsson, S. Andreev, and Y. Koucheryavy, "Analyzing effects of directional deafness on mmWave channel access in unlicensed bands," in *2017 IEEE Globecom Workshops (GC Wkshps)*, pp. 1–7, IEEE, 2017.

[9] T. Cai, J. Fan, and T. Jiang, "Distribution of angles in random packing on spheres," in *2013 J. Mach. Learn. Res. 14*, pp. 1837–1864, 2013.